Vibrated granular media as experimentally realizable Granular Gases

Sean McNamara[1,3] and Eric Falcon[2]

[1] Centre Européen de Calcul Atomique et Moléculaire,
[2] Laboratoire de Physique, École Normale Supérieure de Lyon,
46, allée d'Italie, 69007 Lyon, France
[3] current address: Institute for Computer Applications,
Universität Stuttgart, 70569 Stuttgart, Germany

Summary. We report numerical simulations of strongly vibrated granular materials designed to mimic recent experiments performed both in presence [1] or absence [2] of gravity. We show that a model with impact velocity dependent restitution coefficient is necessary to bring the simulations into agreement with experiments. We measure the scaling exponents of the granular temperature, collision frequency, impulse and pressure with the vibrating piston velocity. As the system changes from a homogeneous gas state at low density to a clustered state at high density, these exponents are all found to decrease continuously with the particle number. In absence of gravity, a loose cluster appears near the upper wall, opposite the piston, and acts as a buffer for fastest particles leading to unexpected non-extensive scaling exponents ; whereas in presence of gravity, the cluster bounces as a single inelastic body. All these results differ significantly from classical inelastic hard sphere kinetic theory and previous simulations, both based on a constant restitution coefficient.

1 Introduction

Granular gases [3] often seem to be the exclusive domain of theory and simulation. For example, the "freely cooling" granular gas [3] is impossible to experimentally realize: even if an experimentalist somehow managed to implement periodic boundaries in all directions, he would still have to contend with energy and time scales that vary over many orders of magnitude. Another frequently studied example of granular gases is the vibrated granular medium. This case is much closer to experiments, because it is relatively simple to put particles in a box and shake them, or drive particles with a vibrating piston. Indeed, there are many experimental [4–6], numerical [6–8], and theoretical [4, 9–11] studies of this system. However, numerous questions remain about the link between experiments on one hand, and theory and simulations on the other. Most numerical and theoretical studies were not intended to be compared with experiments. Therefore, they have parameter values far from

the experimental ones, and none of them predict even the most basic features of the experimental results. For example, numerical and theoretical studies often assume that the vibration frequency is very high so that the shaking wall can be replaced by a thermal boundary. The vibrated granular gas thus attains a steady state. But very high frequencies with an amplitude sufficient to fluidize the granular materials are difficult to attain experimentally; the vibration amplitude in experiments is often a significant fraction of the size of the container. In experiments, the pressure and granular temperature all vary strongly over the period of one vibration cycle. It has therefore been impossible to compare the experimental and numerical results in a meaningful way.

In this paper, we bridge the gap between experiments and numerics by presenting simulations of strongly vibrated granular materials designed to mimic recent experiments [1, 2]. We present the first simulations which resemble the experiments for a large range of parameters. We show that two parameters are especially important for the agreement between experiment and simulation. First of all, an impact velocity dependent restitution coefficient is necessary to bring the simulations into agreement with experiment. Most previous studies consider only constant restitution coefficient [6–8]. Secondly, it is important to explicitly consider the number of particles N. Studying only one value of N or comparing results obtained at different N can lead to interpretive difficulties.

We measure the scaling exponents of the granular temperature, collision frequency, impulse and pressure with the vibrating piston velocity, and find results that differ significantly from classical inelastic hard sphere kinetic theory and previous simulations. Finally, we show that the system undergoes a smooth transition from a homogeneous gas state at low density to a clustered state at high density. Depending on whether gravity is present or not, the transition manifests itself in different ways: due to inelastic collisions (through the restitution coefficient properties), a nearly motionless loose cluster is observed in microgravity with non-extensive scaling properties, whereas a bouncing cluster appears under gravity.

2 Description of the simulations

2.1 The variable coefficient of restitution

The greatest difference between our simulations and the previous numerical studies of vibrated granular media [6–8] is that we use a restitution coefficient that depends on impact velocity. The restitution coefficient r is the ratio between the relative normal velocities before and after impact. In all previous simulations of strongly vibrated granular media, the coefficient of restitution is considered to be constant and lower than 1. However, since a century, it has been shown from impact experiments that r is a function of the impact velocity v [12–16]. Indeed, for metallic particles, when v is large ($v \gtrsim 5$ m/s

[13]), the colliding particles deform fully plastically and $r \propto v^{-1/4}$ [12–14]. When $v \lesssim 0.1$ m/s [13], the deformations are elastic with mainly viscoelastic dissipation, and $1 - r \propto v^{1/5}$ [14–17]. Such velocity-dependent restitution coefficient models have recently shown to be important in numerical [18–23] and experimental [16, 24] studies. Applications include: granular fluidlike properties (convection [19], surface waves [20]), collective collisional processes (energy transmission [21], absence of collapse [16, 22]) and planetary rings [23, 24]. But surprisingly, such model has not yet been tested numerically for strongly vibrated granular media.

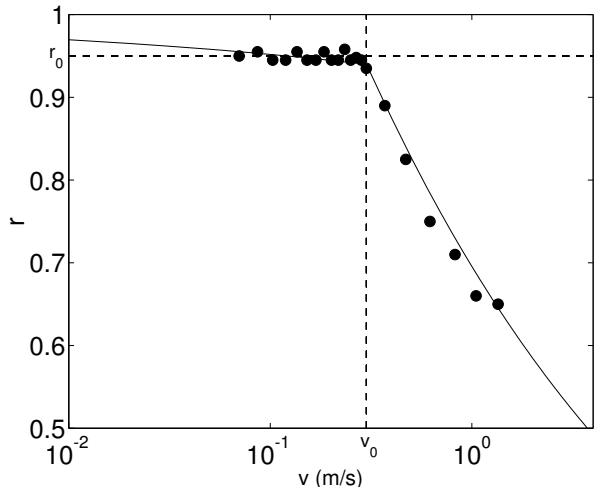

Fig. 1. The restitution coefficient r as a function of impact velocity v, as given in Eq. (1) (solid line). The dashed lines show $v_0 = 0.3$ m/s and $r_0 = 0.95$. Experimental points (•) for steel spheres were extracted from Fig.1 of Ref. [25]

In this paper, we use a velocity dependent restitution coefficient $r(v)$ and join the two regimes of dissipation (viscoelastic and plastic) together as simply as possible, assuming that

$$r(v) = \begin{cases} 1 - (1 - r_0)\left(\frac{v}{v_0}\right)^{1/5}, & v \leq v_0, \\ r_0\left(\frac{v}{v_0}\right)^{-1/4}, & v \geq v_0, \end{cases} \tag{1}$$

where $v_0 = 0.3$ m/s is chosen, throughout the paper, to be the yielding velocity for stainless steel particles [13, 25] for which r_0 is close to 0.95 [25]. Note that $v_0 \sim 1/\sqrt{\rho}$ where ρ is the density of the sphere [13]. We display in Fig. 1 the velocity dependent restitution coefficient of Eq. (1), with $r_0 = 0.95$ and $v_0 = 0.3$ m/s, that agrees well with experimental results on steel spheres from

Ref. [25]. As also already noted by Ref. [13], the impact velocity to cause yield in metal surfaces is indeed relatively small. For metal, it mainly comes from the low yield stress value ($Y \sim 10^9$ N/m^2) with repect to the elastic the Young modulus ($E \sim 10^{11}$ N/m^2). Most impacts between metallic bodies thus involve some plastic deformation.

2.2 The other simulation parameters

The numerical simulation consists of an ensemble of identical hard disks of mass $m \approx 3 \times 10^{-5}$ kg excited vertically by a piston in a two-dimensional box. Simulations are done both in the presence and absence of uniform gravity g. Collisions are assumed instantaneous and thus only binary collisions occur. For simplicity, we neglect the rotational degree of freedom. Collisions with the wall are treated in the same way as collisions between particles, except the wall has infinite mass.

Motivated by recent 3D experiments on stainless steel spheres, 2 mm in diameter, fluidized by a vibrating piston [1], we choose the simulation parameters to match the experimental ones: in the simulations, the vibrated piston at the bottom of the box has amplitude $A = 25$ mm and frequencies $5 \text{ Hz} \leq f \leq 50$ Hz. The piston is nearly sinusoidally vibrated with a waveform made by joining two parabolas together, leading to a maximum piston velocity given by $V = 4Af$. The particles are disks $d = 2$ mm in diameter with stainless steel collision properties through v_0 and r_0 (see Fig. 1). The box has width $L = 20$ cm and horizontal periodic boundary conditions. Since our simulations are two dimensional, we consider the simulation geometrically equivalent to the experiment when their number of layers of particles, $n = Nd/L$, are equal. Hence in the simulation, a layer of particles, $n = 1$, corresponds to 100 particles. We checked that n is an appropriate way to measure the number of particles by also running simulations at $L = 10$ cm and $L = 40$ cm. None of this paper's results depend significantly on L, excpet in Sec. 4.2, where this point is discussed. As in the experiments, the height h of the box depends on the number of particles in order to have a constant difference $h - h_0 = 15$ mm, where h_0 is the height of the bed of particles at rest. Heights are defined from the piston at its highest position.

3 Comparison of simulation and experiment

3.1 The importance of the variable coefficent of restitution

We examine first the dependence of the pressure on the number of particle layers for maximum velocity of the piston $1 \lesssim V \lesssim 5$ m/s ($V = 4Af$). The time averaged pressure at the upper wall is displayed in Fig. 2 as a function of n for various f: from the experiments of Falcon et al. [1] (see Fig. 2a), from our simulations with velocity dependent restitution coefficient $r = r(v)$ proposed

in Eq. (1) (see Fig. 2b), and with constant restitution coefficient $r = 0.95$, often used to describe steel particles (see Fig. 2c), and finally with an unrealistic constant restitution coefficient $r = 0.7$ (see Fig. 2d). Simulations with $r = r(v)$ give results in agreement with the experiments: At constant external driving, the pressure in both Figs. 2a and 2b passes through a maximum for a critical value of n roughly corresponding to one particle layer. For $n < 1$, most particles are in vertical ballistic motion between the piston and the lid. Thus, the mean pressure increases roughly proportionally to n. When n is increased such that $n > 1$, interparticle collisions become more frequent. The energy dissipation is increased and thus the pressure decreases. As we show below in Sec. 4.1, this maximum pressure is not due to gravity because it also appears in simulations with $g = 0$ and $r = r(v)$. Turning our attention to Fig. 2c, we see that setting $r = 0.95$ independently of impact velocity gives pressure qualitatively different from experiments. The difference between Figs. 2b and 2c can be understood by considering a high velocity collision (e.g. $v = 1$ m/s). In Fig. 2b, this collision has a restitution coefficient of $r = r(1\text{ m/s}) \approx 0.7$ (see Fig. 1), whereas in Fig. 2c, r is fixed at 0.95 for all collisions. This means that for equal collision frequencies, dissipation is much stronger for $r = r(v)$ than for $r = 0.95$, because the high velocity collisions dominate the dissipation. Stronger dissipation leads to lower granular temperatures and thus to lower pressures.

We can check this interpretation by changing the constant restitution coefficient to $r = 0.7$ and then comparing it to $r = r(v)$. In these two cases, the high velocity collisions will have roughly the same restitution coefficient. We indeed observed a pressure that decreases for large n for constant $r = 0.7$ (see Fig. 2d). Therefore, surprisingly, constant $r = 0.7$ reproduces more precisely the experimental pressure measurements than constant $r = 0.95$, even though $r = 0.95$ or $r = 0.9$ is often given as the restitution coefficient of steel. Consulting Fig. 1, one can see that $r(v) = 0.7$ is well inside the plastic regime. Therefore, our results suggest that plasticity is much more important than visco-elasticity in vibrated granular media. Although constant $r = 0.7$ gives good agreement with the experiments in Fig. 2, this will not be true in all situations. If the inter-particle collisions were much gentler, the effective coefficient of restitution would rise, and another choice of constant r would be needed. Furthermore, the pressure is just one property of the system. If we look at other property, we see that $r = 0.7$ does not give good results. An example is shown in Fig. 3, where we show three snapshots from three different simulations with $n = 3$ in absence of gravity. When $r = r(v)$, the particles are concentrated in the upper half of the chamber, but they are evenly spread in the horizontal direction (see Fig. 3a). The system is hotter and less dense near the vibrating wall, and colder and denser by the opposite wall. Such a loose cluster has been already observed in microgravity during parabolic flight experiments [26], where grains are agitated with a piston. In contrast, when $r = 0.95$, the particles are uniformly distributed throughout the domain (see Fig. 3b). This occurs because the particle move much faster than the piston,

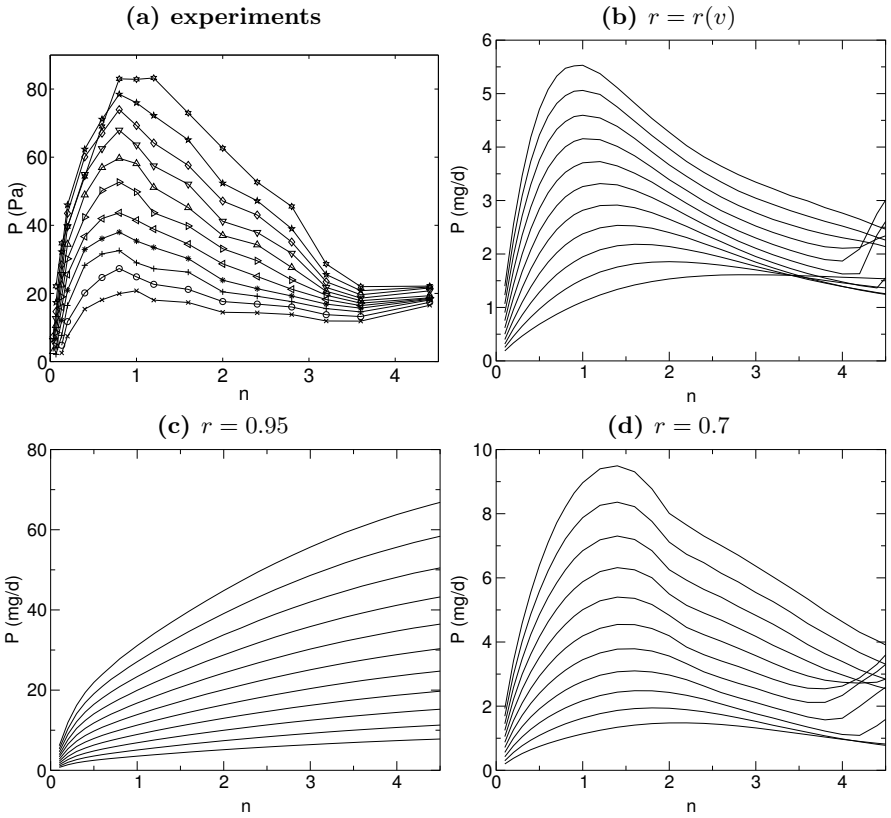

Fig. 2. Time averaged pressure P on the top of the cell as a function of particle layer, n, for various vibration frequencies, f : **(a)** Experimental results from [1] for stainless steel beads 2 mm in diameter, with $A = 25$ mm, $10 \leq f \leq 20Hz$ with a 1 Hz step (from lower to upper) and $h - h_0 = 5$ mm. **(b)** Numerical simulation where the coefficient of restitution is given by Eq. (1), **(c)** Numerical simulation with a coefficient of restitution is 0.95, independent of impact velocity, **(d)** Numerical simulation with a coefficient of restitution is 0.7, independent of impact velocity. The simulations (b) – (d) are 2D with gravity, done for 2 mm disks, with $A = 25$ mm, $10 \leq f \leq 30$ Hz with a 2 Hz step (from lower to upper) and $h - h_0 = 15$ mm. In the simulations, the two-dimensional pressure is given in units of $mg/d \approx 0.15$ Pa·m.

and thus can fill the space left by the descending piston. Finally, when $r = 0.7$, the majority of the particles are confined to a tight cluster, pressed against the upper wall, coexisting with low density region (see Fig. 3c). This instability has been already been reported numerically [27], although for much different parameters (constant restitution coefficient $r = 0.96$, thermal walls, no gravity, and large n). However, nothing like this was ever seen experimentally. Therefore, if one is seeking information about particle positions, $r = 0.7$ gives

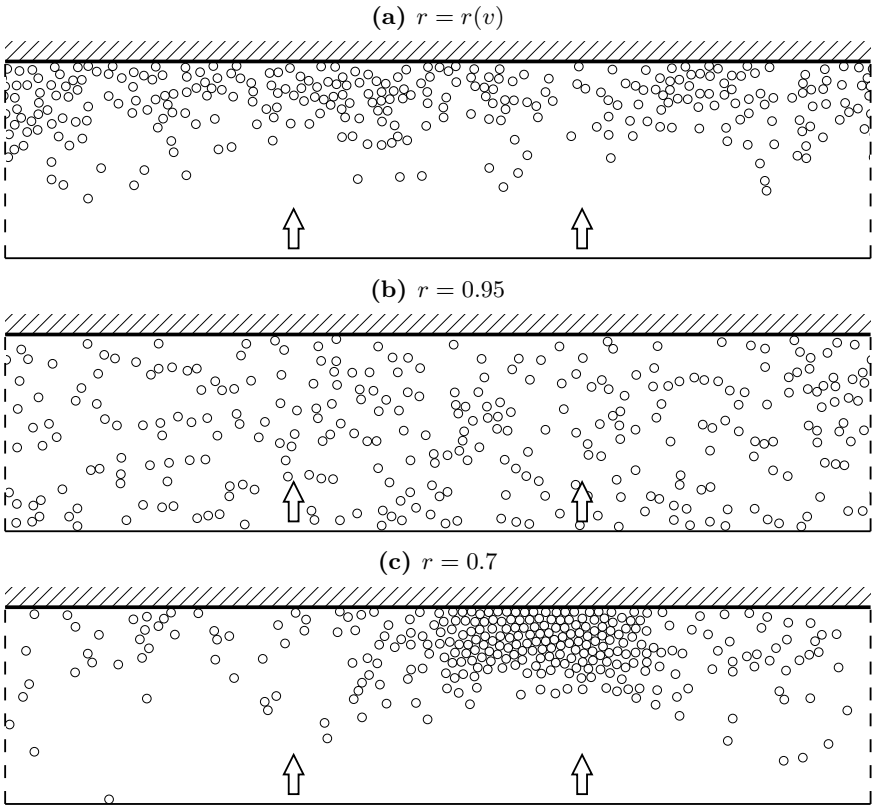

Fig. 3. Snapshots from the simulations with $n = 3$, gravity $g \neq 0$, driving frequency $f = 30$ Hz and $h - h_0 = 15$ mm. The upper wall is stationary, and the lower wall is the piston, which is at its lowest position in all three snapshots. The horizontal boundaries are periodic (indicated by dashed lines). Gravity points downwards. **(a)** $r = r(v)$, as given in Eq. (1), **(b)** constant $r = 0.95$, and **(c)** constant $r = 0.7$. In (c) we see a tight cluster which was not observed in the experiments.

incorrect results even though it gives acceptable results for the pressure. We conclude, therefore, that the only way to successfully describe all the properties in all situations is to use a velocity dependent restitution coefficient model.

3.2 The importance of the particle number

Observations suggest that the the pressure (or granular temperature) of strongly vibrated granular medium is controlled by the piston vibration velocity V. It is important to point out that V is not the only way to characterize the vibration. One could also use the maximum piston acceleration Γ. When

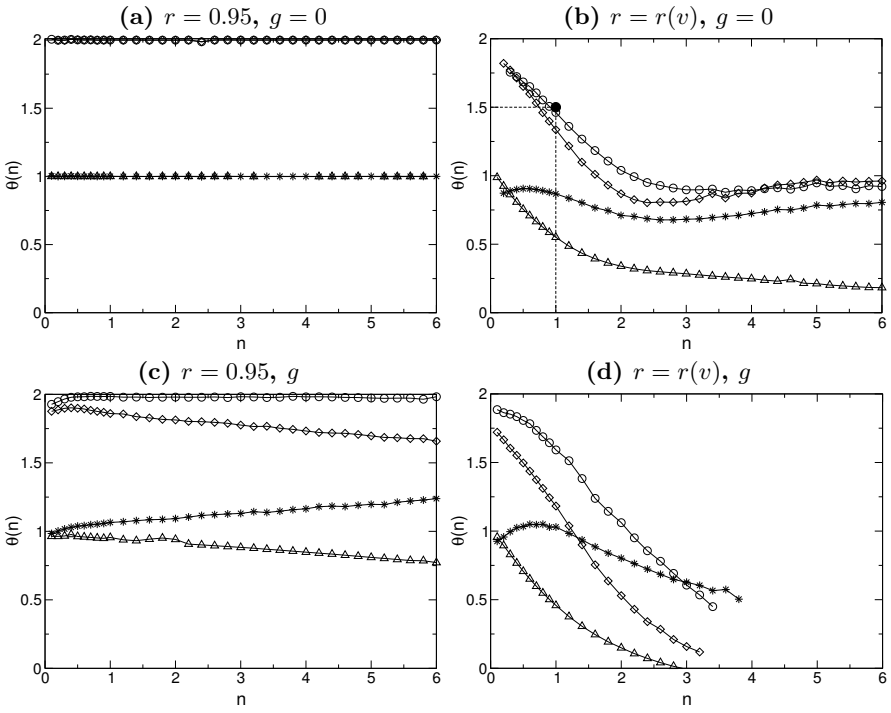

Fig. 4. The exponents θ as a function of n which give the scaling of the granular temperature T ($\Diamond$), collision frequency $C_{\rm upper}$ ($*$), mean impulsions ΔI ($\triangle$) and pressure P ($\circ$). All these quantities are proportional to $V^{\theta(n)}$. Without gravity: **(a)** for $r = 0.95$ and **(b)** for $r = r(v)$. With gravity: **(c)** for $r = 0.95$ and **(d)** for $r = r(v)$. The exponents are obtained by fixing n and performing eleven simulations, varying f from 10 Hz to 30 Hz. Then $\log X$ (where X is the quantity being considered) is plotted against $\log V$. The resulting curve is always nearly a straight line (except for $n > 3$ in (d) – see text), and the exponent is calculated from a least squares fit. The pressure scaling point ($\bullet$) on (b) is from experiment [2] performed in low-gravity. See Fig. 3a (resp. Fig. 3b) for typical snapshots corresponding to $n = 3$, $g \neq 0$ and $r = r(v)$ (resp. $r = 0.95$)

Γ is close to g, it controls the behavior of the system, i.e., adjusting A and f while keeping Γ constant does not change the system's behavior much. But in the simulations presented here, $\Gamma \gg g$, and the system's behavior is controlled by V. This can be checked by multiplying the frequency by 10 while dividing A by 10, thus keeping V the same (while Γ increases by an order of magnitude). Doing so changes the pressure only by about 20%. It is reasonable, therefore, to look for scaling relations in V.

Many authors have postulated that the pressure on the upper wall P (or granular temperature T) is related to the piston velocity V through $P, T \propto$

V^θ. However, it is not clear what the correct "scaling exponent" θ should be. This question has been addressed several times in the past, without a clear resolution of the question [8–11]. For example, kinetic theory [4, 10] and hydrodynamic models [11] predict $T \propto V^2$ whereas numerical simulations [6, 7] or experiments [4–6] give $T \propto V^\theta$, with $1 \leq \theta \leq 2$. These studies were done at single values of n. In this section, we show that it is very important to explicitly consider the dependence of the scaling exponents on n. We also consider the effect of gravity and a variable coefficient of restitution. Doing so enables us to explain and unify all previous works.

At the upper wall, we measured numerically the collision frequency, C_{upper} and the mean impulsion per collision, ΔI for various frequencies of the vibrating wall and numbers of particles in the box, with $r = r(v)$ or with $r = 0.95$, in the presence or absence of gravity. The time averaged pressure on the upper wall can be calculated from these quantities using

$$P = C_{\text{upper}} \Delta I / L \ . \tag{2}$$

(By conservation of momentum, the time averaged pressure on the lower wall is just P plus the weight of the particles Nmg.) The total kinetic energy of the system is also measured to have access to the granular temperature, T. C_{upper}, ΔI, P, and T are all found to fit with power laws in V^θ for our range of piston velocities. Fig. 4 shows θ exponents of C_{upper}, ΔI, P, and T as a function of n. When $g = 0$ and r is constant (see Fig. 4a), we have $P \sim V^2$, $\Delta I \sim V$ and $C_{\text{upper}} \sim V$ for all n. We call these relations the classical kinetic theory scaling. This scaling can be established by simple dimensional analysis when the vibration velocity V provides the only time scale in the system. This is the case for $g = 0$ and r independent of velocity. However, in the experiments, two additional time scales are provided, one by gravity and another by velocity dependent restitution coefficient. Numerical simulations can separate the effects of these two new time scales on the scaling exponents θ. This is done in Fig. 4b [where $g = 0$ but $r = r(v)$] and Fig. 4c [where r is constant but $g \neq 0$]. In both figures, all the exponents become functions of n. However, the time scale linked to $r = r(v)$ leads to much more dramatic departure from the classical scaling. After considering the two time scale separated, let us consider the case corresponding to most experiments, where both gravity and $r = r(v)$ are present (see Fig. 4d). The similarity between this figure and Fig. 4b confirms that the velocity dependent restitution coefficient has a more important effect than the gravity. Furthermore, only the variation of the restitution coefficient on the particle velocity explains the experiment performed in low-gravity [2]. This experiment gives a $V^{3/2}$ pressure scaling (•-mark on Fig. 4b) for $n = 1$ and a motionless clustered state for $n > 2$. Only the simulation with $r = r(v)$ can reproduce these results (see Fig. 4b) whereas constant r simulations leads to the classical scaling ($P \propto V^2$, see Fig. 4a) and only a gaseous state for all n shown in the figure.

As shown in Fig 4, it is thus very important to explicitly consider the dependence of θ on n. In all cases, except the unrealistic case of Fig. 4a, θ

depends on n. To our knowledge, the only experiment [1] to systematically investigate this effect shows that $T \propto V^{\theta(n)}$, with θ continuously varying from $\theta = 2$ when $n \to 0$, as expected from kinetic theory, to $\theta \simeq 0$ for large n due to the clustering instability. These experiments [1] performed under gravity (shown in Fig. 5) are well reproduced by the simulations of Fig. 4d. In both cases, the observed pressure and granular temperature scaling exponents strongly decrease with n.

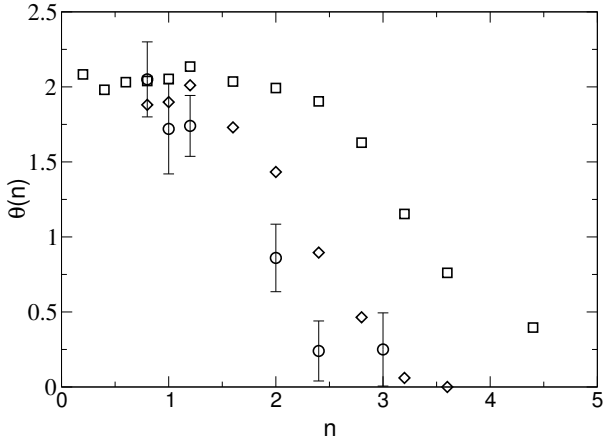

Fig. 5. Experimental data performed under gravity from Ref. [1]: The exponents $\theta(n)$ of time averaged pressure (□) (see Fig. 2a), and kinetic energy extracted from density profile (○) or volume expansion (◊) measurements. These data should be compared with the simulations of Fig. 4d.

We finish this section by noting two curious facts about Fig. 4. First of all, in Fig. 4b [$g = 0$ and $r = r(v)$], $\theta \approx 1$ for the pressure and temperature when $n > 2$. This is the sign of new robust scaling regime where $P, T \propto V$, which is the subject of Sec. 4.1. Secondly, in Fig. 4d [$g \neq 0$ and $r = r(v)$], the scaling exponents are not shown for $n \geq 3$, because the dependence of P, T C_{upper} and ΔI on V is no longer a simple power law. (More precisely, we do not plot a point on Fig. 4 when $|\log X_{\text{observed}} - \log X_{\text{fitted}}| \geq 0.25$ for any of the eleven simulations used to calculate the exponent – see caption.) The power law breaks down because there is a resonance between the time of flight of the cluster under gravity and the vibration period. This is the subject of Sec. 4.2.

4 Effects of clustering ($n > 2$ or 3)

4.1 Clustering without gravity

In this section, we examine the situation concerning realistic particles [$r = r(v)$] in microgravity ($g = 0$). At high enough density, a loose cluster is formed that resembles Fig. 3a (even though $g \neq 0$ in Fig. 3a), and we noted that $P \propto V$ for $n > 2$ (see Fig. 4b). We would like to know if there is some simple physical explanation for this aparently robust scaling relation. To investigate this question, we present in Fig. 6 the dependence of P on V, n and $h - h_0$.

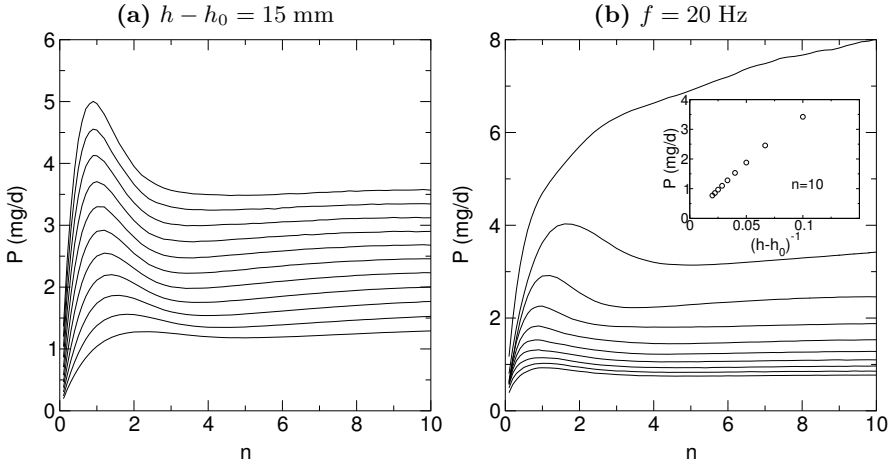

Fig. 6. Time averaged pressure P on the top of the cell as a function of particle layer, n: **(a)** for various vibration frequencies: $f = 10$ Hz (lowest curve) to $f = 30$ Hz (uppermost curve) with steps of 2 Hz; **(b)** for various heights: $h - h_0 = 5$ mm (uppermost curve) to $h - h_0 = 50$ mm (lowest curve) with steps of 5 mm. Inset: P vs. $(h - h_0)^{-1}$ for $n = 10$ and 10 cm $\leq h - h_0 \leq 50$ cm. Simulations were done with $g = 0$ and $r = r(v)$.

Fig. 6a shows the same quantities as Fig. 2, except that the scale of the x-axis has changed: instead of $0 < n < 4.5$, we show $0 < n < 10$. Note that Fig. 6a concerns the same situation as in Fig. 2b, except here the gravity has been "turned off". Thus it is not surprising that for $n < 3$, the two figures are almost the same: after a rapid increase of the pressure for small n, there is a maximum pressure near $n \approx 1$. But for $n > 3$, the figures are different: in Fig. 2b, the pressure decreases as particles are added, but in Fig. 6a the pressure is nearly independent of n. Therefore, when $g = 0$, the pressure is not changed by adding more particles, as long as there are already enough particles present. Considering now the dependence of P on V, we note that the evenly spaced curves in Fig. 6a suggest that $P \propto V$. We have confirmed

this proportionality by calculating the pressure scaling exponent and checking that it remains close to 1. (The exponent for $n < 6$ has already been shown in Fig. 4b.) In Fig. 6b, we examine how changing $h - h_0$ affects the pressure. We see that the pressure is independent of n for $n > 3$ and $h - h_0 \geq 10$, with the pressure decreasing as the height increases. Examining the dependence of the pressure on $h - h_0$ shows that $P \propto (h - h_0)^{-1}$. (For example, see the inset in Fig. 6b.) Thus, the pressure obeys the simple non-extensive relation

$$P \propto \frac{N^0 V^1}{h - h_0} \tag{3}$$

Recall that this relation concerns high enough number of realistic particles in microgravity. Therefore, this pressure scaling of Eq. (3) may be observable in microgravity experiments. One complication is that in microgravity experiments, one does not usually agitate the grains with a piston (except very recently [26]) – it is much simpler to shake a box of fixed size [2].

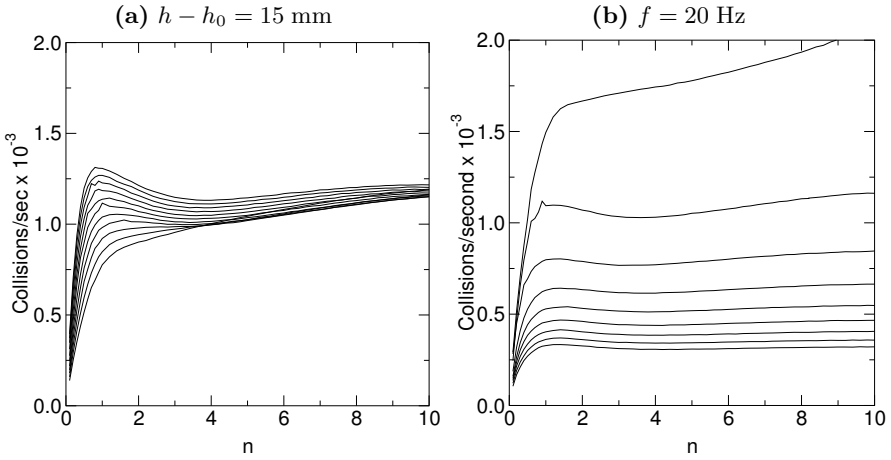

Fig. 7. The particle-piston collision rate C_{lower} as a function of particle layer, n: **(a)** for various vibration frequencies: $f = 10$ Hz (lowest curve) to $f = 30$ Hz (uppermost curve) with steps of 2 Hz; **(b)** for various heights: $h - h_0 = 10$ mm (uppermost curve) to $h - h_0 = 50$ mm (lowest curve) with steps of 5 mm. Simulations are done with $g = 0$ and $r = r(v)$.

In Fig. 3a, we observe that the majority of particles remain in a loose cluster pushed against the stationary wall, opposite the piston. Only those particles that "evaporate" from the cluster are struck by the piston. The evaporation rate can be estimated from the rate of collisions between the piston and the particles C_{lower}. This collision rate has a very curious behavior, as shown in Fig. 7. As can be seen from Fig. 7a, C_{lower} is roughly independent

of n and V when $n > 3$. This behavior hold for other values of $h - h_0$, as can be seen from Fig. 7b. Thus, at high enough density, the collision frequency on the vibrating wall is found to be

$$C_{\text{lower}} \propto \frac{N^0 V^0}{h - h_0}. \tag{4}$$

We now present a simple model and a physical interpretation of the unexpected scaling of Eq. (3) for such a loose cluster. We suppose that the cluster against the stationary wall has a granular temperature independent of both the number of particles N and the vibration velocity V. The granular temperature is independent of N and V because the impact velocity dependent restitution coefficient acts as a kind of "granular thermostat". As one can see from Eq. (1) or Fig. 1, when the typical particle velocity v is greater than v_0, $r(v)$ is small, and energy is dissipated rapidly. On the other hand, when $v < v_0$, $r(v)$ is nearly unity and energy dissipation is slow. Thus, in a weakly forced cluster, like the one found at the stationary wall, $T \sim v^2$ will be near v_0^2, independent of the strength of the forcing and the size of the cluster.

Since the granular temperature of the cluster is independent of N and V, so is the flux F_{evap} of grains "evaporating" from the cluster and moving towards the piston. If all the grains that evaporate from the cluster reach the piston, then we have $C_{\text{lower}} = F_{\text{evap}} \propto N^0 V^0$. In their collision with the piston, the grains acquire an upwards velocity proportional to V. Thus the flux of momentum entering the system at the piston is $VC_{\text{lower}} \propto N^0 V^1$. Since momentum is conserved, the flux of momentum leaving the system through the stationary wall must have the same value. But the time averaged pressure P is just the time averaged momentum flux divided by the area of the upper wall. Thus our model predicts $P \propto N^0 V^1$, in agreement with Eq. (3).

This theory also explains why P and C_{lower} are inversely proportional to $h - h_0$. When a particle evaporates from the cluster, it must travel a certain distance before it encouters the piston. This distance increases with $h - h_0$ and thus the particle's travel time also increases. During its voyage, the evaporated particle could be struck by another particle that has just encountered the piston. If this happens, both particles are scattered back into the cluster. Thus the evaporated particle never reaches the piston. If we assume that the probability of an evaporated particle being scattered back into the cluster is independent of time, the number of particles reaching the piston is inversely proportional to $h - h_0$.

This explanation can be checked by looking at the probability density of vertical (y) velocities parallel to the direction of vibration. In Fig. 8, we show these density functions. Note the assymmetry of the distibution's positive and negative wings. The edge of the positive wing increases linearly with V whereas the negative wing extends much more slowly. The reason for this is that the positive wing is populated by particles which have just been struck by the piston. Their velocity is thus proportional to V. On the other hand,

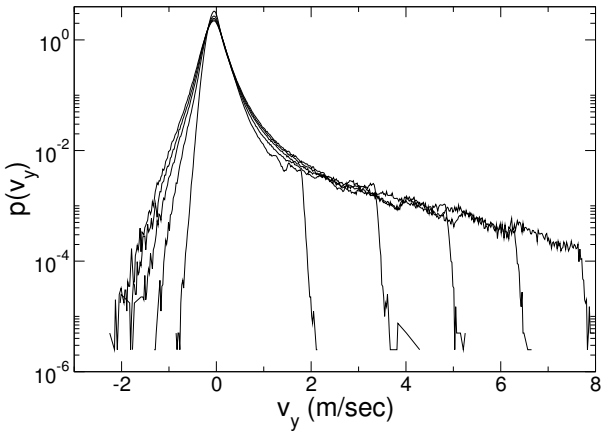

Fig. 8. The probability density function of the vertical velocities at high density, for $n = 5$, $r = r(v)$, and $g = 0$. The driving frequencies are $f = 10$ Hz (narrowest distribution) to $f = 50$ Hz (broadest distribution) with steps of 10 Hz.

the negative wing is due to fluctuations in the cluster. The negative wing thus expands slowly because of the "thermostat" effect described above.

We conclude by emphasizing that this effect can only be seen with the velocity dependent restitution coefficient. If one uses a constant restitution coefficient, one obtains $P \propto V^2$, no matter the value of r.

4.2 Clustering with gravity

In this section, we consider the situation that applies to most of the experiments, i.e. realistic particles [$r = r(v)$] under gravity. We will show that the relatively simple situation described in the previous section is complicated by the presence of gravity. Under gravity, the loose cluster will not remain near the upper wall (unless f is large), but will fall downwards towards the piston. At certain values of f, $h - h_0$ and large enough n, a resonance occurs between the driving frequency and the time of flight of the particles, leading to a cluster that bounces back and forth between the piston and the wall. As f increases, however, we recover the situation found in the previous section.

In Fig. 9, we show two pictures from the experiments of Ref. [1]. At low densities, the particles move like atoms in a gas (Fig. 9a). At higher densities, a cluster forms that bounces up and down on the piston (Fig. 9b). This cluster was observed only for certain frequencies, densities and container heights. It was not possible to establish a criterion for the existence of the cluster based on the experimental data. Both of these behaviors are reproduced in the simulations (Fig. 10). Therefore, the simulations should give insight into the origin of the bouncing cluster.

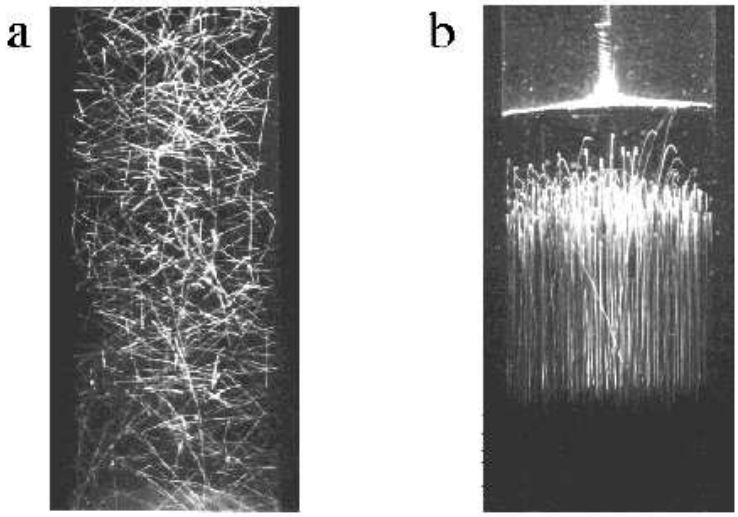

Fig. 9. Photographs of particle trajectories from the experiments of [1], showing the cluster at high densities. In both pictures $f = 20$ Hz and $A = 40$ mm. The number of layers of particles is **(a)** $n = 1$ **(b)** $n = 4$. The driving piston is at the bottom (not visible), the inner diameter of the tube being 52 mm.

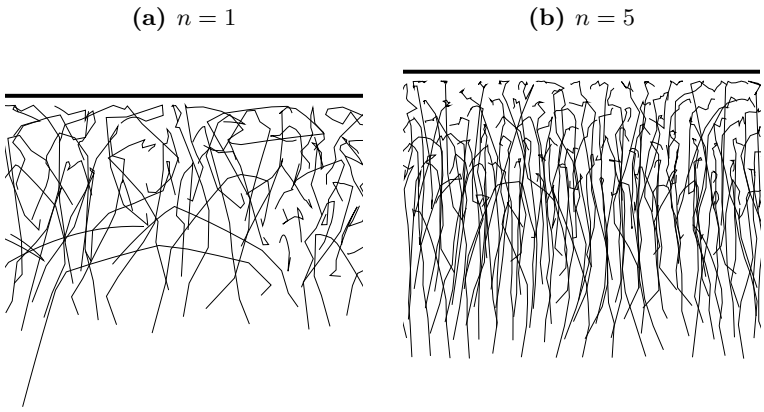

Fig. 10. Particle trajectories from the simulations with $f = 20$ Hz, $A = 25$ mm, $r = r(v)$, and $h - h_0 = 15$ mm. The number of layers of particles is **(a)** $n = 1$ and **(b)** $n = 5$. The containers have different sizes, because the size of the container is increased as more particles are added, as was done in the experiments.

We first examine the relation between P and V in a case where the bouncing cluster is observed. One does not obtain the simple scaling in Eq. (3) for the pressure. Instead, one obtains a much more complicated relation between P and V. Indeed, as we show in Fig. 11, the pressure displays two maxima as a function of V. These maxima correspond to the bouncing cluster shown

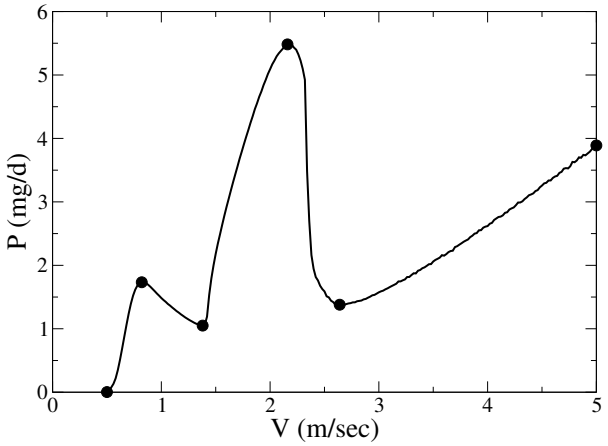

Fig. 11. Pressure as a function of the piston velocity, $V = 4Af$, for $n = 6$, $r = r(v)$, $h - h_0 = 15$ mm under gravity. Simulations where done for $f = 5$ Hz to $f = 50$ Hz with steps of 0.2 Hz. The dots mark the particular frequencies shown in Fig. 12.

in Figs 9b and 10b. The bouncing cluster transports momentum very effectively between the piston and the wall. When the bouncing cluster disappears at $n < 3$, the maxima also disappear. These maxima make it impossible to describe the relation between the pressure and the forcing by a simple power law. This is the reason why there are no points on Fig. 4d for $n > 3$.

Unlike the other results of this paper, Fig. 11 changes significantly when L and N are changed while holding n fixed. When L and N are both divided by two, the first maximum moves to $V \approx 1$ m/sec and the second maximum disappears. When L and N are doubled, the second maximum moves to near $V \approx 1.4$ m/sec. Therefore, the results of this section should not be considered as a systematic investigation of the resonance, but rather a descriptive introduction. The resonance is sensitive to L because it can involve horizontal collective motions of the particles, not just vertical ones. Indeed, for $L = 40$ cm, one can observe waves similar to those discussed in [20].

To investigate the origins of the bouncing cluster, we show in Fig. 12 the position of the piston and the approximate location of the cluster as a function of time for various driving frequencies. The frequencies are chosen to correspond to the maxima and minima of the pressure, and are indicated by the large points in Fig. 11. At very low frequencies (Fig. 12a), the pressure

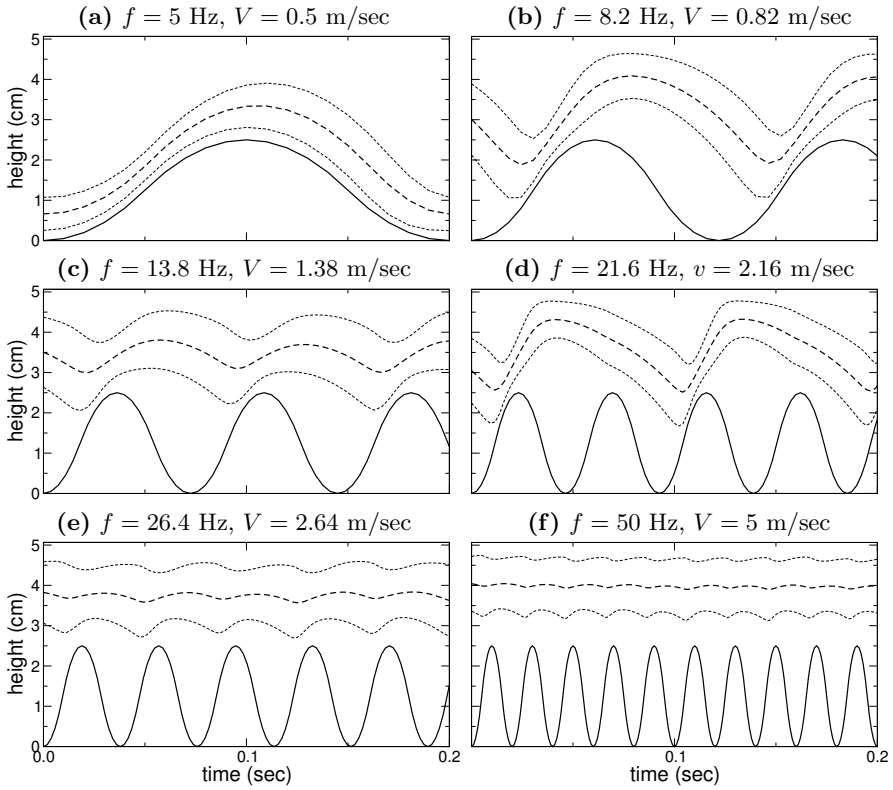

Fig. 12. The motion of the grains under gravity at various vibration frequencies during 0.2 seconds, for $n = 6$, $h - h_0 = 25$ mm and $r = r(v)$. In all plots, the vertical axis is height, with the lower boundary at the piston's lowest point, and the upper boundary being the upper wall of the container. Solid line shows the position of the piston. The heavy dotted line shows the height $y_{\rm cm}$ of the center of mass. The upper and lower thin dotted lines show $y_{\rm cm} + \sigma_{\rm cm}$ and $y_{\rm cm} - \sigma_{\rm cm}$ respectively, where $\sigma_{\rm cm}$ is the standard deviation of the particle heights at a given instant. The majority of the particles are thus contained between the two thin dotted lines.

vanishes because no particles hit the top of the container. The cluster bounces on the vibrating plate. As the piston velocity increases, the cluster flies higher and higher until it strikes the top. The pressure reaches a first maximum near $V = 0.82$ m/s (Fig. 11) where there is a first resonance between the time of flight of the cluster and the vibration period. These two times are such that the cluster lands on the piston just when the piston is at its maximum upwards velocity (Fig. 12b). Note that a large number of particles descend below the piston's maximum height. Then as the piston rises, it sweeps up all the particles, increasing the density of the cluster. On the other hand, as the cluster falls from the stationary wall, it slowly expands.

As the piston velocity increases further, the pressure decreases, because the cluster lands on the piston when it is near its maximum height (Fig. 12c). Then the pressure rises to a new maximum near $V = 4Af = 2.2$ m/s (Fig. 11) because there is a second resonance: the cluster's flight time is equal to two piston cycles (Fig. 12d). Note that the frequencies of these two resonances ($f = 8.2$ Hz and $f = 21.6$ Hz) are not related by a simple factor of 2. The reason for this is that the time of flight of the cluster depends in a complicated way on the piston velocity. Comparing Figs. 12b and 12d, one can see that the velocity of the cluster when it leaves the piston is close to V, but the time it takes the cluster to fall back from the upper wall onto the vibrating is roughly independent of V. Note also that the collisions between the cluster and the piston or wall takes a finite time, as can be seen by comparing the times of the minima of $y_{\rm cm} + \sigma_{\rm cm}$, $y_{\rm cm}$, and $y_{\rm cm} - \sigma_{\rm cm}$ in Fig. 12b. All of these effects exclude a simple resonance condition for the pressure maxima. The resonant frequencies depend on g and $h - h_0$. The resonant frequencies are proportional to $g^{1/2}$ but decrease for as $h - h_0$ is increased. The resonant frequencies are not sensitive to changing n, as long as n is sufficiently large.

At higher driving frequencies (Fig. 12e and Fig. 12f), the center of mass of the particles changes very little over one cycle, and there are no more resonances. In fact, setting $g = 0$ changes Fig. 12f very little. The reason for this is that average particle kinetic energy is much larger than gh, so gravity is irrelevant. Higher order resonances, (where the cluster's flight time equals three or more vibration periods) are not observed. These resonances are probably not observed because there is not enough time for the particles to fall below the piston's highest point. Thus, the piston does not gather up all the particles into a single dense cluster, but rather acts to disperse the cluster. For example, imagine that the driving frequency is suddenly doubled in Fig. 12d just at the moment when the cluster starts its descent from the wall. When the cluster arrives at the piston, perhaps a half of the particles will be swept up by one vibration cycle, and a half in the next cycle. This is how energetic forcing breaks up clusters.

5 Conclusions

In Sec. 3, we brought simulations as close as possible to the experiments. To bring simulations into agreement with the experiments, it is essential to use a velocity dependent coefficient of restitution. It is especially important to take into account plastic deformations that cause the restitution coefficient to decrease rapidly with increasing impact velocity. Indeed, the restitution coefficient for strongly vibrated steel spheres is very far from the constant values of $r = 0.95$ or $r = 0.9$ that are often cited in simulations as typical for steel spheres. We also noted that it is very important to take into account the number of particle layers n. The dependence of the pressure P on the piston velocity V changes with n. It is not accurate to speak of "a" scaling exponent

for the pressure in terms of V: this exponent depends continuously on n, and does not exist at high density ($n > 3$) under gravity, due to the clustering instability.

In Sec. 4, we investigated this question of clustering. When there is no gravity, a loose cluster forms against the stationary wall opposite the vibrating piston. Due to the velocity dependent restitution coefficient, this cluster acts as a buffer for fastest particles, and leads to a simple non-extensive scaling $P \propto N^0 V$. Unlike the case with gravity, the scaling holds for a wide range of parameters. We discussed the origin the scaling, and remarked that it should be observable in microgravity experiments. We also studied the effect of clustering in the presence of gravity. In this case, the clusters give a very complicated behavior, because there are interactions between the period of vibration and the flight time of the cluster. Finally, if the vibration frequency is strong enough, the cluster can be broken up, because the cluster-piston collision time becomes longer than vibration period.

Acknowledgments
We thank Stéphan Fauve for fruitful discussions. The authors gratefully acknowledge the hospitality of the ENS-Lyon physics department which made this collaboration possible.

References

1. E. Falcon, S. Fauve, and C. Laroche. *Experimental Study of Granular Gas Fluidized by Vibrations*, pages 244–253. Volume 564 of Pöschel and Luding [3], 2001. E. Falcon, S. Fauve and C. Laroche. *Eur. Phys. J. B.* **9**:183, 1999; *J. Chim. Phys.* **96**:1111,1999.
2. E. Falcon et al. *Phys. Rev. Lett.*, **83**:440, 1999.
3. T. Pöschel and S. Luding, editors. *Granular Gases.* Number **564** in Lectures Notes in Physics. Springer-Verlag, Berlin, 2001.
4. S. Warr, J. M. Huntley, and G. T. H. Jacques. *Phys. Rev. E*, **52**:5583, 1995.
5. X. Yang and D. Candela. *Phys. Rev. Lett.*, **85**:298, 2000. R. D. Wildman, J. M. Huntley and D. J. Parker. *Phys. Rev. E*, **63**:061311, 2001.
6. S. Luding et al. *Phys. Rev. E*, **49**:1634, 1994.
7. S. Luding, H. J. Herrmann, and A. Blumen. *Phys. Rev. E*, **50**:3100, 1994. S. Luding. *Phys. Rev. E*, **52**:4442, 1995. H. J. Herrmann and S. Luding. *Continuum Mech. and Thermodyn.*, **10**:189, 1998.
8. S. McNamara and S. Luding. *Phys. Rev. E*, **58**:813, 1998.
9. J. M. Huntley. *Phys. Rev. E*, **58**:5168, 1998.
10. V. Kumaran. *Phys. Rev. E*, **57**:5660, 1998.
11. J. Lee. *Physica A*, **219**:305, 1995.
12. C. V. Raman. *Phys. Rev.*, **12**:442, 1918. D. Tabor. *Proc. Roy. Soc. A*, **192**:247, 1948. W. Goldsmith. *Impact*, Arnold, London, 1960.
13. K. L. Johnson. *Contact Mechanics.* Cambridge Univ. Press, Cambridge, 1985.
14. L. Labous, A. D. Rosato, and R. N. Dave. *Phys. Rev. E*, **56**:5717, 1997.
15. G. Kuwabara and K. Kono. *Jap. J. of Appl. Phys.*, **26**:1230, 1987.

16. E. Falcon, C. Laroche, S. Fauve, and C. Coste. *Eur. Phys. J. B*, **3**:45, 1998. See also references therein.
17. J.-M. Hertzsch, F. Spahn, and N. V. Brilliantov. *J. Phys. II (Paris)*, **5**:1725, 1995. J. Schäfer, S. Dippel and D. E. Wolf. *J. Phys. I (Paris)*, **6**:5, 1996. S. Luding et al. *Phys. Rev. E*, **50**:4113, 1994.
18. N. V. Brilliantov and T. Pöschel. *Phys. Rev. E*, **61**:5573, 2000.
19. C. Salueña, T. Pöschel, and S. E. Esipov. *Phys. Rev. E*, **59**:4422, 1999.
20. C. Bizon et al. *Phys. Rev. Lett.*, **80**:57, 1998.
21. T. Pöschel and N. V. Brilliantov. *Phys. Rev. E*, **63**:021505, 2001.
22. D. Goldman et al. *Phys. Rev. E*, **57**:4831, 1998.
23. H. Salo, J. Lukkari, and J. Hänninen. *Earth, Moon, and Planets*, **43**:33, 1988. F. Spahn, U. Schwarz and J. Kurths. *Phys. Rev. Lett.*, **78**:1596, 1997. H. Salo. *Granular Gases*, pages 330–349. In Pöschel and Luding [3], 2001.
24. F. G. Bridges, A. Hatzes, and D. N. C. Lin. *Nature*, **309**:333, 1984. A. Hatzes, F. G. Bridges and D. N. C. Lin. *Mont. Not. R. Astr. Soc.*, **231**:1091, 1988. K. D. Supulver, F. G. Bridges and D. N. C. Lin. *Icarus*, **113**:188, 1995. M. Higa, M. Arakawa and N. Maeno. *Icarus*, **44**:917, 1996.
25. J. M. Lifshitz and H. Kolsky. *J. Mech. Phys. Solids*, **12**, 1964.
26. E. Falcon, S. Fauve, P. Evesque, F. Palencia, C. Chabot, Y. Garrabos, and D. Beysens, 2003. Unpublished.
27. M. Argentina, M. G. Clerc, and R. Soto. *Phys. Rev. Lett.*, **89**:044301, 2002. See also M. Argentina, M. G. Clerc and R. Soto in this book.